ACS APPLIED MATERIALS & INTERFACES

Research Article

www.acsami.org

Cutting and Unzipping Multiwalled Carbon Nanotubes into Curved Graphene Nanosheets and Their Enhanced Supercapacitor Performance

Huanwen Wang,[†] Yalan Wang,[†] Zhongai Hu,[‡] and Xuefeng Wang*[,†]

[†]Department of Chemistry, Tongji University, Shanghai 200092, China

[‡]College of Chemistry and Chemical Engineering, Northwest Normal University, Lanzhou 730070, China

ABSTRACT: We report a remarkable transformation of multiwalled carbon nanotubes (MWCNTs) to curved graphene nanosheets (CGN) by the Hummers method. Through this simple process, MWCNTs can be cut and unzipped in the transverse and longitudinal directions, respectively. The as-obtained CGN possess the unique hybrid structure of 1D nanotube and 2D graphene. Such a particular structure together with the improved effective surface area affords high specific capacitance and good cycling stability during the charge−discharge process when used as supercapacitor electrodes. The electrochemical measurements show that CGN exhibit higher capacitive properties than pristine MWCNTs in three different types of aqueous electrolytes, 1 M KOH, 1 M H_2SO_4, and 1 M Na_2SO_4. A specific capacitance of as high as 256 F g^{-1} at a current density of 0.3 A g^{-1} is achieved over the CGN material. The improved capacitance may be attributed to high accessibility to electrolyte ions, extended defect density, and increased effective surface area. Meanwhile, this high-yield production of graphene from low cost MWCNTs is important for the scalable synthesis and industrial application of graphene. Furthermore, this novel CGN nanostructure could also be promisingly applied in many fields such as nanoelectronics, sensors, nanocomposites, batteries, and gas storage.

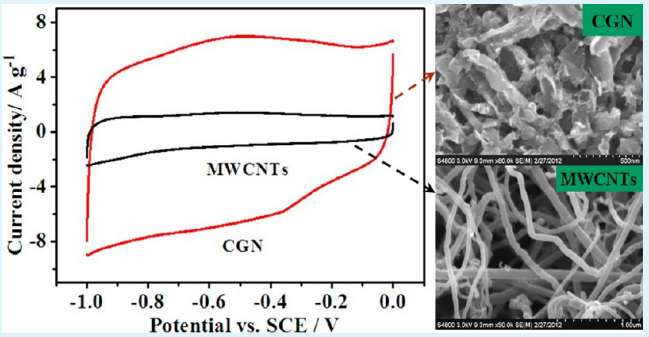

KEYWORDS: *multiwalled carbon nanotubes, graphene, the Hummers method, supercapacitors, energy storage*

1. INTRODUCTION

As a new class of energy storage devices, supercapacitors are now attracting intensive attention because of their unique advantages including long cycle life, superior reversibility, high power density, and low maintenance cost.[1,2] These features meet the demand in, e.g., hybrid electric vehicles, portable electronics, and energy management systems.[3] Generally, the supercapacitor performance is mainly determined by electrode materials. In recent years, carbon nanotubes (CNTs) have been investigated as promising electrode materials for supercapacitors due to their well-defined nanostructure, high electrical conductivity, and chemical stability.[4] However, typical CNTs are prepared with lengths in the range of micrometers and are aggregated into macroscopically entangled ropes or masses, which impede ion transport in the inner tube of CNT, especially for multiwalled carbon nanotubes (MWCNTs) and thereby limit any improvement in the specific capacitance (15−200 F g^{-1}) of supercapacitors.[5−7] To fully realize the unique properties of CNTs, methods for modification at the macroscopic scale need to be developed.

In a recent application of CNT manipulation, shorter fragments and nanoribbons have been obtained through cutting and unzipping of CNTs. A number of methods have been practiced to cut long CNTs to short lengths, including ball-milling,[8] cryogenic crushing,[9] solid-state reaction,[10,11] selective etching in molten nitrate,[12] fluorination,[13] chemical oxidation,[14] and electrochemical preparation.[15] It has been found that short segments of CNTs obtained by transverse cutting display much better performance than that of pristine CNTs for application in Li-ion batteries[16] and solar cells.[17] Longitudinal unzipping of CNTs results in the formation of graphene nanoribbons by means of plasma etching,[18] oxidative treatment,[19,20] electrochemical approach,[21] potassium vapor followed by protonation,[22] and catalytic hydrogenation.[23] More recently, a facile and clean method is used to synthesize few-layer N-doped graphene nanoribbons via thermal expansion of N_2 molecules inserted in surface defects and in the hollow core of the concentric tubes.[24] Experimental evidence suggests that the CNTs with open ends produced by acid treatments can exhibit higher electrochemical reactivity than those of CNTs with closed ends.[25−27] Despite this progress, one-step cutting and unzipping of CNTs in transverse and longitudinal directions is still a challenging task, owing to many associated problems of various nature, including complex procedures and difficult

Received: September 15, 2012
Accepted: November 13, 2012
Published: November 13, 2012

manipulation. Meanwhile, it is reasonable to expect that shortening and unravelling of CNTs would lead to a much enhanced performance for applications in electrochemical energy storage. Therefore, seeking for the effective strategies to simultaneously cut and split CNTs remains a major topic of interest.

Here, a modified Hummers method[28] is applied to cut and unzip CNTs. Taking low cost into account, we select MWCNTs as the raw materials. The results indicate that MWCNTs have been transversely cut and longitudinally unzipped, resulting in the formation of curved graphene nanosheets (CGN). The obtained CGN could possess the partial tube structure with graphene morphology. More importantly, this hybrid structure could improve significantly the accessible area since both the outer and inner wall of CNTs is available. When the CGN serve as electrode materials, high specific capacitance and excellent cycling stability are achieved for supercapacitor application.

2. EXPERIMENTAL SECTION

2.1. Synthesis of Samples. MWCNTs were used as received from Chengdu Organic Chemicals (Chengdu, P.R. China). The remaining chemicals were purchased from Sigma-Aldrich and used as received.

CGN were synthesized by a two-step process, including oxidation and reduction. MWCNTs were oxidized according to the modified Hummers method. Typically, 2 g of MWCNTs and 1 g of sodium nitrate were mixed with 92 mL of concentrated sulfuric acid (98%) in a 500 mL flask. The mixture was stirred for 1 h within an ice bath. Six g of potassium permanganate was added to the suspension under vigorous stirring. The rate of addition was carefully controlled to keep the reaction temperature lower than 20 °C. After removal of the ice bath, the mixture was stirred at 35 °C for 1 h. Then, 92 mL of deionized water was slowly added with vigorous agitation. The diluted suspension was stirred for 30 min. At the end, 20 mL of H_2O_2 (30%) and 280 mL of deionized water were added to the mixture. The mixture was washed and centrifuged with 10% HCl and deionized water for several times. The washing process was repeated until the pH of the solution became neutral. After dry under vacuum, oxidized MWCNTs (O-MWCNTs) were obtained as a gray powder. The final yield of O-MWCNTs from the pristine CNT is ca. 78%.

The O-MWCNTs (100 mg) were dispersed in 100 mL of water by ultrasonic treatment 1 h. Then 500 mg of $NaBH_4$ was slowly added to the mixture, with stirring for 24 h under room temperature. Finally, the solid sample was collected after washing with ethanol and deionized water and vacuum-dried at 60 °C to obtain the CGN material.

2.2. Materials Characterization. The products were characterized by field emission scanning electron microscopy (FESEM; Philips XSEM30, Holland) and transmission electron microscope (TEM; JEOL, JEM-2010, Japan). The structure of the samples was examined by X-ray diffraction (XRD; Philips PC-APD) with Cu Kα radiation (λ = 1.5418 Å) operating at 40 kV, 60 mA. The components of materials were measured by a Nicolet Nexus 670 FT−IR instrument. Raman spectra were collected using a 514 nm laser with RM100 under ambient conditions, with a laser spot size of about 1 mm. The nitrogen adsorption−desorption isotherms were measured at 77 K by an automatic adsorption instrument (Tristar3000, Micromeritics).

2.3. Preparation of Electrodes. To evaluate the electrochemical properties of the samples, working electrodes were fabricated as described in our previous paper.[29] The as-prepared samples, acetylene black and polytetrafluoroethylene (PTFE) binder were mixed in a weight ratio of 75:20:5, using ethanol as the solvent to yield a paste. Addition of acetylene black could enhance the conductivity of active materials and further increase the electrochemical utilization of an electrode. This paste was incorporated into nickel foam or graphite electrode (1 cm × 1 cm), and the mass of active material in the working electrode was 2.0 mg.

2.4. Evaluation of Electrochemical Properties. A typical three-electrode experimental cell equipped with a working electrode, a platinum foil counter electrode, and an SCE reference electrode was used for measuring the electrochemical properties of the working electrode. Electrochemical measurements were carried out in 1 M KOH, 1 M H_2SO_4, and 1 M Na_2SO_4 aqueous electrolytes. Cyclic voltammetry (CV) and galvanostatic charge−discharge were carried out on a CHI660B electrochemical working station. The specific capacitance was calculated by $C = I \times t/(V \times m)$, where I is the discharging current, t is the discharging time, V is the potential drop during discharge, and m is the mass of active material in a single electrode.

3. RESULTS AND DISCUSSION

3.1. Synthesis of the CGN Material. It is well-known that graphite can be effectively oxidized to form graphite oxide by the Hummers method. Graphite oxide could disperse in aqueous solutions as individual layers, which can then be reduced and deoxygenated with chemical or thermal processes.[30] During oxidation, oxygen atoms are included into the carbon network. This leads to O-containing surface groups and defects, which induce various degrees of deformation or damage to the honeycomb lattice. Considering that both CNT and graphite are composed of graphene, we try to select the Hummers method to cut and unzip CNTs to prepare the CGN. As shown in Figure 1, the preparing process involves two steps, including oxidation with the Hummers method and reduction with $NaBH_4$.

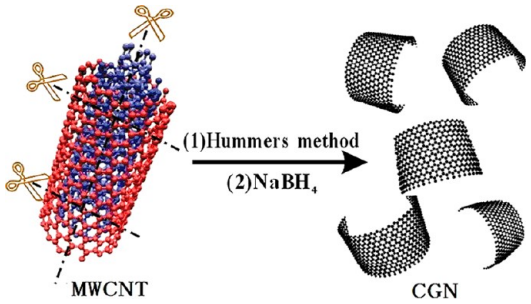

Figure 1. The preparation of the CGN material by combining the Hummers method and subsequent reduction with $NaBH_4$.

Cutting and unzipping of the MWCNTs were confirmed by FESEM and TEM. Figure 2a and c show FESEM images of commercially produced MWCNTs. It can be seen that these MWCNTs are curved and entangled and have diameters ranging from 40−100 nm and lengths in the micrometer range. After the processing of the Hummers method, the MWCNTs present a remarkable morphology transformation. As shown in the low magnification image (Figure 2b), it is clearly observed that CNTs are successfully cut in the transverse direction, yielding shorter fragments with lengths of hundreds of nanometers. From the high magnification image (Figure 2d), we find that these shorter CNTs have been unzipped along the longitudinal direction, and graphene sheet structures could be found. However, they do not form a totally flat graphene sheet but display a tubelike structure. TEM images indicate that the obtained CGN are unwrapped into graphene sheets, but the partial tube structure could still be identified (Figure 3a, c). The interplanar spacing of the pristine MWCNTs is measured to be 0.34 nm (Figure 3b), corresponding to the crystal lattice

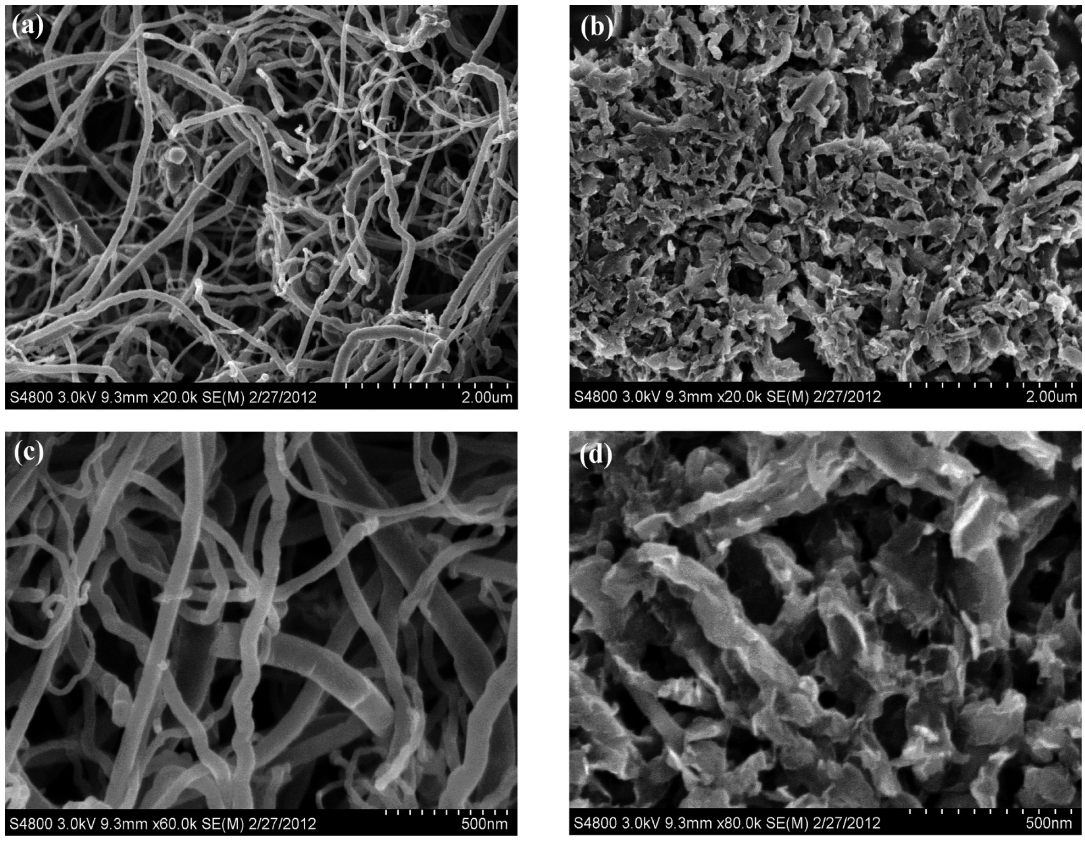

Figure 2. FESEM images of the MWCNTs (a, c) and CGN (b, d).

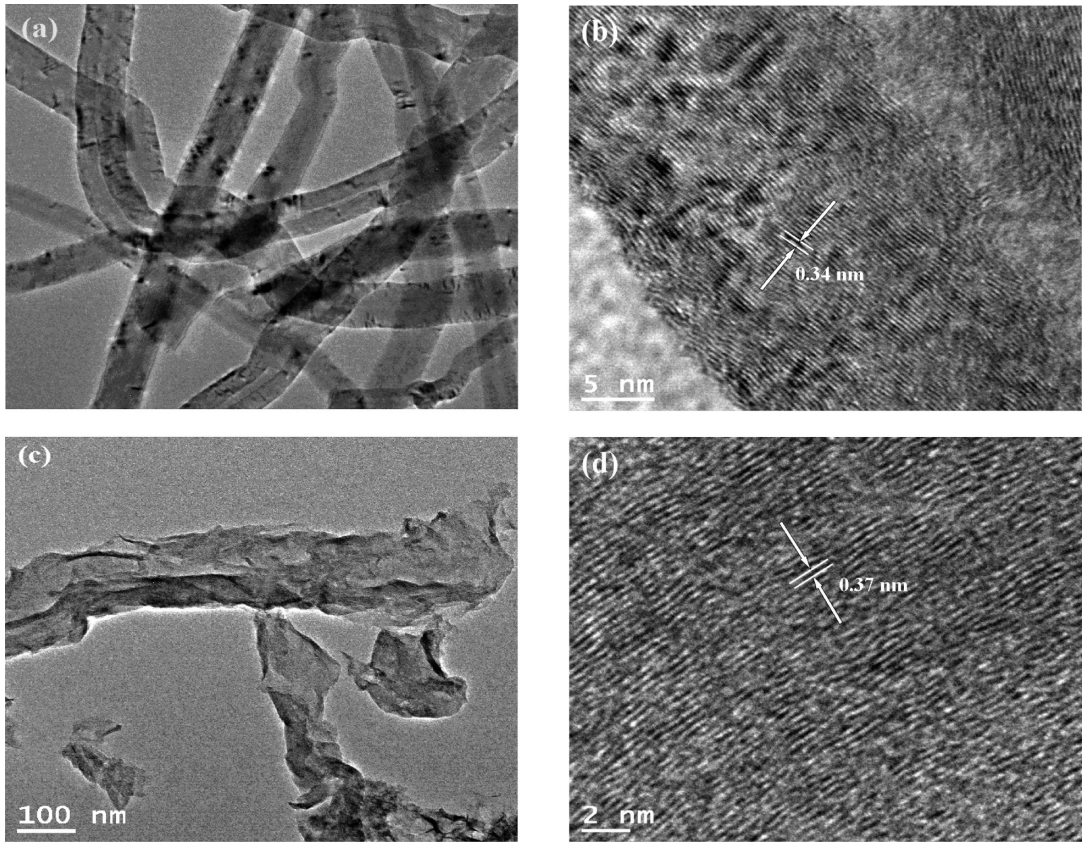

Figure 3. TEM images of the MWCNTs (a, b) and CGN (c, d).

dx.doi.org/10.1021/am302000z | *ACS Appl. Mater. Interfaces* 2012, 4, 6827−6834

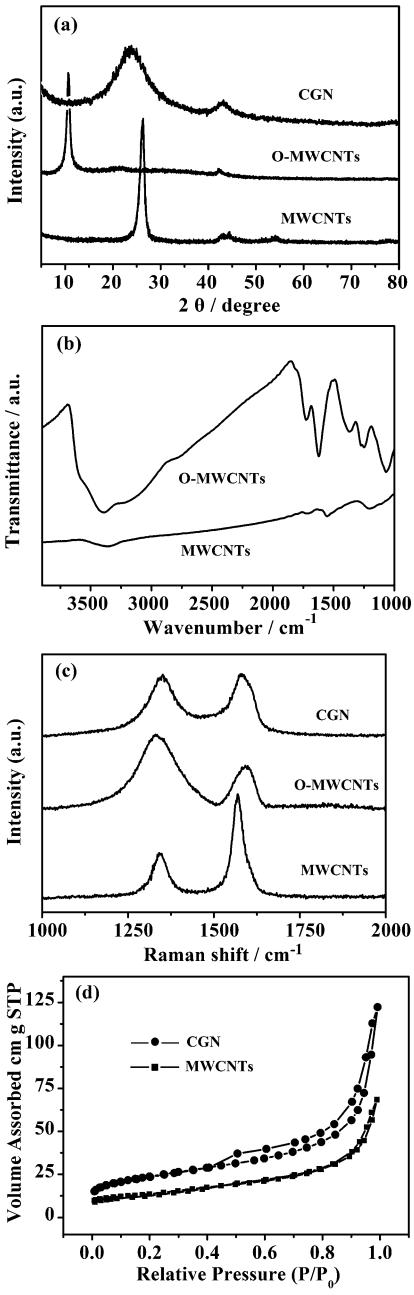

Figure 4. XRD patterns (a), Raman spectra (b), FTIR spectra (c), and N_2 adsorption (d) of MWCNTs, O-MWCNTs, and CGN.

distance of multiwalled CNTs. After cutting and unzipping, the interplanar spacing is up to 0.37 nm (Figure 3d).

3.2. Material Characterization. The crystal phase and structure information of the products were obtained by XRD, FTIR, Raman, and the N_2 adsorption−desorption. Oxidation usually generates large amounts of oxygen functionalities, which can be intercalated in the c-plane of the graphene layers and correspondingly increase the interlayer spacing. This process is monitored by XRD (Figure 4a), as evidenced by a peak at 2θ = 10.3° with the basal spacing of 8.6 Å. After reduction with $NaBH_4$, this peak completely disappeared, and a very broad peak at around 23.2° was observed, corresponding to an interlayer spacing of about 3.7 Å. It is slight larger than *d*-spacing (3.4 Å) of CNTs, indicating the presence of residual oxgen-containing functional groups or other structural defects.

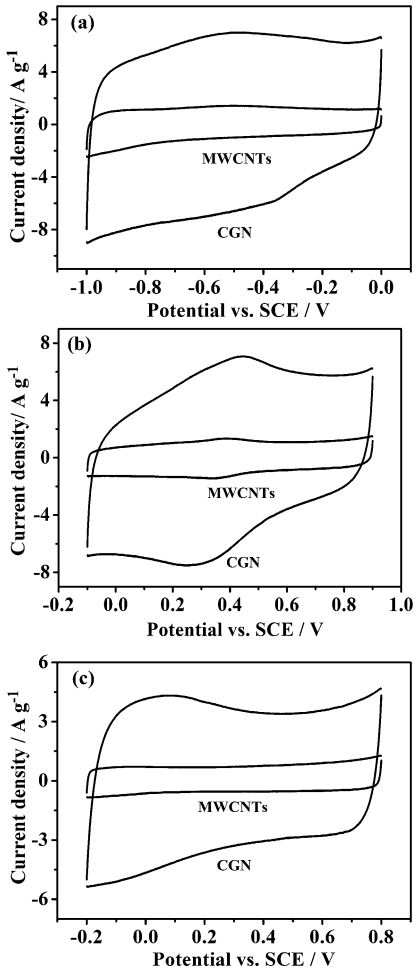

Figure 5. CV curves of MWCNTs and CGN at 50 mV s^{-1} in 6 M KOH (a), 1 M H_2SO_4 (b), and 1 M Na_2SO_4 (c).

This is in agreement with the result of TEM. The sawtooth-shaped broad reflection at 43.1° indicates that CGN exhibit turbostratic disorder (Figure 4a). The existence of remaining oxygen functionalities and disorder improves high accessibility to electrolyte ions.

FTIR spectrum of the O-MWCNTs (Figure 4b) shows two absorption peaks with very strong intensity located at 3400 cm^{-1} and 1624 cm^{-1}, corresponding to O−H stretching and bending vibration, respectively. The other oxygen-containing functional groups are revealed by the bands at 1725, 1065, 1245, and 1375 cm, which correspond to C═O in COOH, C−O, C−OH, and C−O−C, respectively. This result is consistent with a graphite oxide structure.[31] We also performed Raman analysis (Figure 4c), to investigate further the structure of the O-MWCNT and CGN. After oxidation, the ratio of the intensities of the D and G bands (I_D/I_G) increases from 0.45 to 1.88. This change suggests that strong oxidation causes a decrease in the average size of the sp^2 domains after the cutting and unzipping process. The oxygen functional groups in the O-MWCNT can be almost removed by a chemical reduction,[32,33] and the conjugated G network (sp^2 carbon) will be re-established. However, the size of the re-established G network is smaller than that of the pristine MWCNTs, which show the presence of structural defects. These defects are in favor of capacitance enhancement. The N_2 adsorption−desorption isotherm of the as-prepared CGN exhibits type IV character-

dx.doi.org/10.1021/am302000z | ACS Appl. Mater. Interfaces 2012, 4, 6827−6834

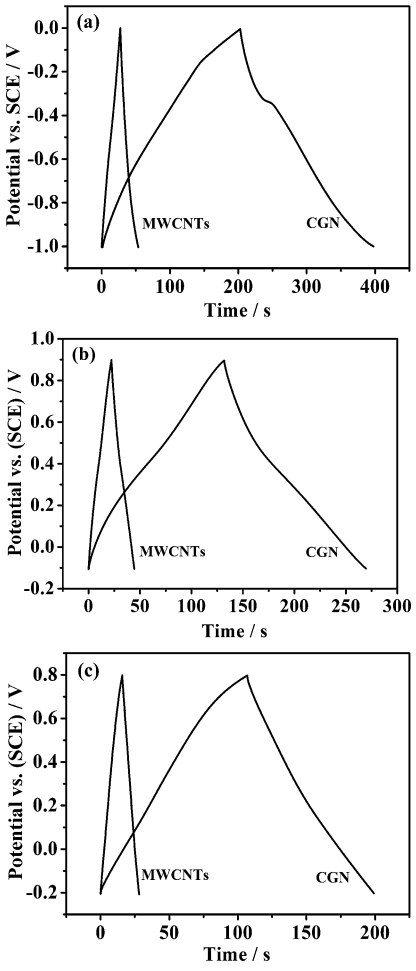

Figure 6. Galvanostatic charge–discharge curves of MWCNTs and CGN at 1 A g^{-1} in 6 M KOH (a), 1 M H_2SO_4 (b), and 1 M Na_2SO_4 (c).

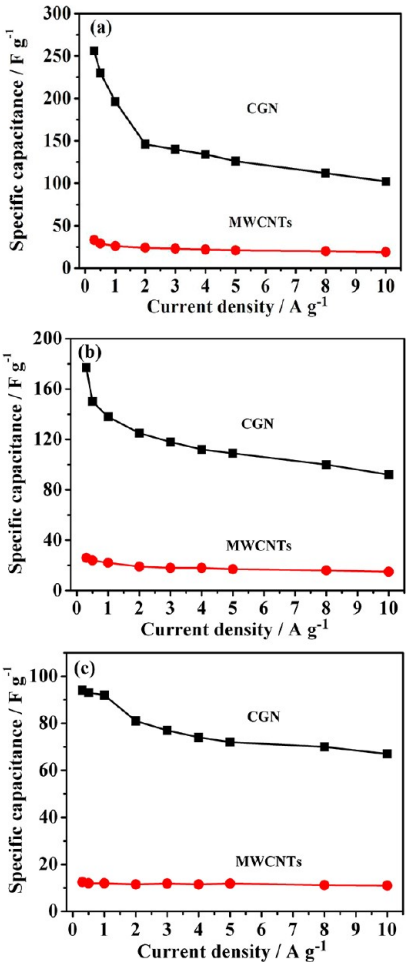

Figure 7. Specific capacitance of MWCNTs and CGN at different current density of 0.3 A g^{-1} to 10 A g^{-1} in 6 M KOH (a), 1 M H_2SO_4 (b), and 1 M Na_2SO_4 (c).

istics (Figure 4d), which are indicative of the presence of relatively large pores in the sample. It is worth noting that the Brunauer–Emmett–Teller (BET) specific surface area of CGN (85 m^2 g^{-1}) is much higher than that of MWCNTs (47 m^2 g^{-1}). The surface area enhancement can serve as a strong evidence for successful cutting and unzipping of MWCNT and further boost capacitive performance. On the whole, these above results confirm that the oxidation of CNTs is similar to that of natural graphite.[34,35]

3.3. Electrochemical Characterization. CV and galvanostatic charging–discharging measurements were performed to compare pristine MWCNTs and the CGN material at 50 mV s^{-1} scan rate in 1 M KOH, 1 M H_2SO_4, and 1 M Na_2SO_4, and the results are shown in Figure 5. The specific capacitance is proportional to the area under the CV curve, which is much larger for CGN than for MWCNTs in three different types of aqueous electrolytes (Figure 5). Figure 6 shows galvanostatic charging–discharging curves of MWCNTs and CGN at 1 A g^{-1} current density. The increase in the charging time represents the higher capacitance of the CGN. The specific capacitance is shown as a function of the current density in Figure 7. The specific capacitance of CGN is up to 256 F g^{-1} at a current density of 0.3 A g^{-1} in 1 M KOH solution. In contrast, the specific capacitance of the MWCNTs is only 33 F g^{-1} at 0.3 A g^{-1} in the same electrolyte (Figure 7a). In 1 M H_2SO_4 and 1 M Na_2SO_4 electrolyte (Figure 7b, c), the CGN shows better rate capability than that in 1 M KOH. At a high current density of 10 A g^{-1}, there is more than 71% retention in the capacitance relative to 0.3 A g^{-1} in 1 M Na_2SO_4. Meanwhile, we find that the nature of the electrolyte strongly influences capacitive properties of CGN. Usually, the functional groups attached to CGN are more chemically active in alkali or acidic electrolytes where redox reactions occur, which is evidenced from the shapes of CV curves (Figure 7a, b). In 1 M Na_2SO_4 electrolyte, the capacitance is mainly originated from double layer capacitance. However, the combination of electric double-layer capacitance and faradaic capacitance is responsible for high specific capacitance in 1 M KOH or H_2SO_4 solution.

Because a long cycle life is one of key factors for supercapacitor application, an endurance test was conducted using galvanostatic charging–discharging cycles at 5 A g^{-1} (Figure 8). In 1 M KOH, the CGN electrode can keep 99% of the initial value over 5000 cycles (Figure 8a). In 1 M H_2SO_4, the specific capacitance of the sample increases with cycling numbers. After a 5000-cycle test, the specific capacitance reaches a high value of 158 F g^{-1}, which is higher than its initial value (116 F g^{-1}) (Figure 8b). In 1 M Na_2SO_4, the decay in specific capacitance after a 5000-cycle test is only 3% (Figure 8c). These results indicate that the CGN exhibit excellent cycling stability.

3.4. Discussion. Andreas Hirsch[36] reviewed the opening mechanism of the CNTs where in the initial rate-determining

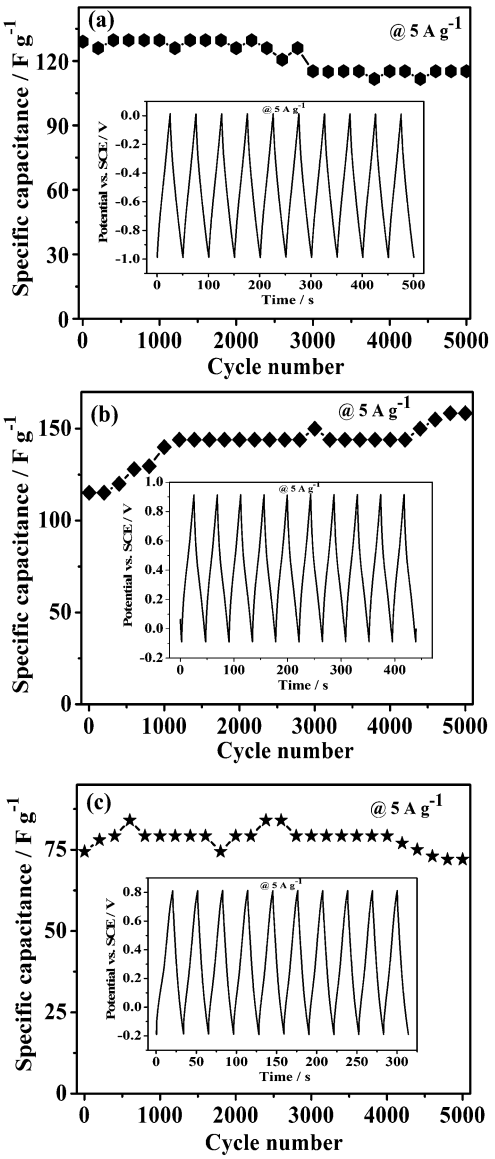

Figure 8. Evolution of the specific capacitance of CGN versus the number at 5 A g^{-1} in 6 M KOH (a), 1 M H_2SO_4 (b), and 1 M Na_2SO_4 (c).

step a manganate ester is formed by the addition to an unsaturated bond of the nanotube side wall. The subsequent oxidation is facilitated by the dehydrating medium and leads to an opened diketone defect flanked by β, γ double bonds. There are two different points between the Hummers method and the Tour method. The first is the existence of sodium nitrate in the Hummers method that is known to have strong oxidizability to carbon materials such as CNTs in concentrated sulfuric acid. The second is the different temperature performance. Usually, the Tour method needs higher temperature (70 °C) to unzip CNTs completely.[20,26] However, the mixture materials could explode upon heating in 7 wt %/vol $KMnO_4/H_2SO_4$ solution.[37] For the safety reason, CNT oxidation should be performed at room temperature for the best. Therefore, in our system, MWCNTs can be cut and unzipped in the transverse and longitudinal direction, respectively. In addition, edge states significantly affect the electronic properties and chemical activity of the graphene nanoribbons. From Raman and XRD patterns, we find that rough or imperfect edges are formed within the CGN, which is in agreement with previous oxidation of MWCNTs.[19,20]

Table 1. Summary of Electrochemical Measurements Reported for CNTs Supercapacitor Electrodes

technique	nature of CNT	electrolyte	capacitance (F g^{-1})	ref (year)
spray deposition	film/multi, single	0.1 M H_2SO_4	77/155	38 (2009)
CVD	film/ multilayered	NaCl	79.8	39 (2010)
CVD	film/single	$EABF_4$/PC	32	40 (2009)
CVD	film/single	LiCl	41.4	41 (2010)
DC arc discharge	powder/ single	7.5 M KOH	180	42 (2001)
electrostatic spray	powder/multi	1 M H_2SO_4	108	43 (2006)
CVD	film/multi	6 M KOH	20	44 (2005)
KOH activation	powder/multi	4 M H_2SO_4	62	45 (2006)
HNO_3 oxidation	powder/ double	0.5 M H_2SO_4	54	46 (2009)
CVD	film/single	1 M $LiClO_4$/ PC	35	47 (2011)
layer-by-layer assembly	film/multi	1 M H_2SO_4	159	48 (2009)
printable technique	film/single	H_3PO_4	120	49 (2009)
controlled oxidation	powder/ single	Et_4NBF_4/PC	114	50 (2010)
printable technique	paper/single	1 M $LiPF_6$	200	51 (2009)
the Tour method	powder/multi	3 M NaOH	165	27 (2011)
the Hummers method	powder/multi	1 M KOH	256	this work

Usually, the capacitive behaviors of CNTs are dependent on several factors, including surface modification, defect density, electronic conductivity, diffusion resistance to electrolyte ions, and effective surface area. Much work has shown applications of CNTs in supercapacitors. Table 1 summarizes some of the results that have been obtained to date with CNTs as a supercapacitor electrode material. CNTs are often regarded as the choice of a high-power electrode material because of their good electrical conductivity and readily accessible surface area. However, the low energy density is a concern. Although single-walled carbon nanotubes (SWCNTs) have higher specific capacitance than MWCNTs due to larger surface area per unit mass,[38−43] the high cost of SWCNTs limits their feasibility for device applications.[27] As shown in Table 1, different strategies have been used to activate and functionalize CNTs to improve the energy density. Despite significant progress, however, most of the fabrication processes of CNT electrodes are either too delicate,[44−47] which makes them less viable for large-scale industrial applications, or display thin film structure,[48−51] which yields much lower volumetric density than powders. Particularly, the capacitance value of CGN is even higher than that of exfoliated carbon nanotubes prepared by the Tour′ method (Table 1).

Based on these considerations, the goal of the present work is to use a simple and scalable fabrication technique to optimize the supercapacitor performance of CNT electrodes. First, the MWCNTs are directly cut and unzipped by the Hummers method. Second, reduction with $NaBH_4$ restores π-conjugated

network. As a result, the obtained CGN exhibit much higher supercapacitor performance in comparison with the pristine MWCNTs due to the following factors: 1) The oxidation process and subsequent reduction allow for the formation of some oxgen-containing functional groups, which could generate pseudocapacitance and other structural defects, which can improve electrolyte ionic accessibility. 2) Insertion/extraction of electrolyte ions is easier into/from short CNTs as compared to long CNTs because of the transverse cutting. 3) The longitudinal unzipping increases effective surface area, which would release more electroactive sites for fast electrochemical reactions. 4) The tube structure can exploit the full advantages of 1D carbon nanotube and 2D graphene structure, which could prevent the restacking problem of graphene sheets, and in the mean time, provide a path for rapid electron transport. Taken together, we conclude that the Hummers method can effectively improve the supercapacitor performance of CNTs-based electrodes.

4. CONCLUSIONS

In summary, MWCNTs are successfully cut and unzipped by the Hummers method. Interestingly, the oxidation of MWCNTs is similar to that of natural graphite. The obtained CGN display the tube structure. CV and galvanostatic charging-discharging measurements were performed to characterize these materials as supercapacitor electrodes. Relative to pristine MWCNTs, the CGN show much higher capacitance and have outstanding capacity retention on cycling.

AUTHOR INFORMATION

Corresponding Author

*E-mail: xfwang@tongji.edu.cn.

Notes

The authors declare no competing financial interest.

ACKNOWLEDGMENTS

The authors gratefully acknowledge the financial support offered by NSFC (20973126, 21173158), STCSM (10PJ1409600), and NSFC (20963009, 21163017).

REFERENCES

(1) Xie, K.; Qin, X.; Wang, X.; Wang, Y.; Tao, H.; Wu, Q.; Yang, L.; Hu, Z. *Adv. Mater.* **2012**, *24*, 347−352.
(2) Guan, C.; Li, X.; Wang, Z.; Cao, X.; Soci, C.; Zhang, H.; Fan, H. J. *Adv. Mater.* **2012**, *24*, 4186−4190.
(3) Chen, Y. L.; Hu, Z. A.; Chang, Y. Q.; Wang, H. W.; Zhang, Z. Y.; Yang, Y. Y.; Wu, H. Y. *J. Phys. Chem. C* **2011**, *115*, 2563−2571.
(4) Izadi-Najafabadi, A.; Yamada, T.; Futaba, D. N.; Yudasaka, M.; Takagi, H.; Hatori, H.; Iijima, S.; Hata, K. *ACS Nano* **2011**, *5*, 811−819.
(5) An, K. H.; Kim, W. S.; Park, Y. S.; Moon, J. M.; Bae, J. D.; Lim, S. C.; Lee, Y. S.; Lee, Y. H. *Adv. Funct. Mater.* **2001**, *11*, 387−392.
(6) Yang, C. M.; Kim, Y. J.; Endo, M.; Kanoh, H.; Yudasaka, M.; Iijima, S.; Kaneko, K. *J. Am. Chem. Soc.* **2007**, *129*, 20−21.
(7) Frackowiak, E.; Béguin, F. *Carbon* **2001**, *39*, 937−950.
(8) Rubio, N.; Fabbro, C.; Herrero, M. A.; de la Hoz, A.; Meneghetti, M.; Fierro, J. L. G.; Prato, M.; Vázquez, E. *Small* **2011**, *7*, 665−674.
(9) Lee, J.; Jeong, T.; Heo, J.; Park, S. H.; Lee, D. H.; Park, J. B.; Han, H.; Kwon, Y. N.; Kovalev, I.; Yoon, S. M.; Choi, J. Y.; Jin, Y. W.; Kim, J. M.; An, K. H.; Lee, Y. H.; Yu, S. G. *Carbon* **2006**, *44*, 2984−2989.
(10) Wang, X. X.; Wang, J. N. *Carbon* **2008**, *46*, 117−125.
(11) Wang, X. X.; Wang, J. N.; Su, L. F.; Niu, J. J. *J. Mater. Chem.* **2006**, *16*, 4231−4234.
(12) Wang, Y.; Zhang, J.; Zang, J.; Ge, E.; Huang, H. *Corros. Sci.* **2011**, *53*, 3764−3770.
(13) Gu, Z.; Peng, H.; Hauge, R. H.; Smalley, R. E.; Margrave, J. L. *Nano Lett.* **2002**, *2*, 1009−1013.
(14) Ziegler, K. J.; Gu, Z.; Peng, H.; Flor, E. L.; Hauge, R. H.; Smalley, R. E. *J. Am. Chem. Soc.* **2005**, *127*, 1541−1547.
(15) Shinde, D. B.; Pillai, V. K. *Chem.—Eur. J.* **2012**, *18*, 12522−12528.
(16) Wang, X. X.; Wang, J. N.; Chang, H.; Zhang, Y. F. *Adv. Funct. Mater.* **2007**, *17*, 3613−3618.
(17) Kalita, G.; Adhikari, S.; Aryal, H. R.; Umeno, M.; Afre, R.; Soga, T.; Sharon, M. *Appl. Phys. Lett.* **2008**, *92*, 123508−123511.
(18) Jiao, L.; Zhang, L.; Wang, X.; Diankov, G.; Dai, H. *Nature* **2009**, *458*, 877−880.
(19) Kosynkin, D. V.; Higginbotham, A. L.; Sinitskii, A.; Lomeda, J. R.; Dimiev, A.; Price, B. K.; Tour, J. M. *Nature* **2009**, *458*, 872−876.
(20) Wang, Y.; Shi, Z. X.; Yin, J. *J. Phys. Chem. C* **2010**, *114*, 19621−19628.
(21) Shinde, D. B.; Debgupta, J.; Kushwaha, A.; Aslam, M.; Pillai, V. K. *J. Am. Chem. Soc.* **2011**, *133*, 4168−4171.
(22) Kosynkin, D. V.; Lu, W.; Sinitskii, A.; Pera, G.; Sun, Z.; Tour, J. M. *ACS Nano* **2011**, *5*, 968−974.
(23) Elías, A. L.; Botello-Méndez, A. R.; Meneses-Rodríguez, D.; González, V. J.; Ramírez-González, D.; Ci, L.; Muñoz-Sandoval, E.; Ajayan, P. M.; Terrones, H.; Terrones, M. *Nano Lett.* **2010**, *10*, 366−372.
(24) Morelos-Gómez, A.; Vega-Díaz, S. M.; González, V. J.; Tristán-López, F.; Cruz-Silva, R.; Fujisawa, K.; Muramatsu, H.; Hayashi, T.; Mi, X.; Shi, Y.; Sakamoto, H.; Khoerunnisa, F.; Kaneko, K.; Sumpter, B. G.; Kim, Y. A.; Meunier, V.; Endo, M.; Muñoz-Sandoval, E.; Terrones, M. *ACS Nano* **2012**, *6*, 2261−2272.
(25) Fang, W. C.; Huang, J. H.; Chen, L. C.; Su, Y. O.; Chen, K. H.; Sun, C. L. *Electrochem. Solid-State Lett.* **2006**, *9*, 5−8.
(26) Long, D.; Li, W.; Qiao, W.; Miyawaki, J.; Yoon, S. H.; Mochida, I.; Ling, L. *Chem. Commun.* **2011**, *47*, 9429−9431.
(27) Wang, G.; Ling, Y.; Qian, F.; Yang, X.; Liu, X. X.; Li, Y. *J. Power Sources* **2011**, *196*, 5209−5214.
(28) Hummers, W. S.; Offeman, R. E. *J. Am. Chem. Soc.* **1958**, *80*, 1339.
(29) Wang, H. W.; Hu, Z. A.; Chang, Y. Q.; Chen, Y. L.; Wu, H. Y.; Zhang, Z. Y.; Yang, Y. Y. *J. Mater. Chem.* **2011**, *21*, 10504−10511.
(30) Stankovich, S.; Piner, R. D.; Chen, X.; Wu, N.; Nguyen, S. T.; Ruoff, R. S. *J. Mater. Chem.* **2006**, *16*, 155−158.
(31) Stankovich, S.; Dikin, D. A.; Piner, R. D.; Kohlhaas, K. A.; Kleinhammes, A.; Jia, Y.; Wu, Y.; Nguyen, S. T.; Ruoff, R. S. *Carbon* **2007**, *45*, 1558−1565.
(32) Wang, Y.; Shi, Z. X.; Yin, J. *Polymer* **2011**, *52*, 3661−3670.
(33) Wang, Y.; Shi, Z. X.; Yin, J. *ACS Appl. Mater. Interfaces* **2011**, *3*, 1127−1133.
(34) Dreyer, D. R.; Park, S.; Bielawski, C. W.; Ruoff, R. S. *Chem. Soc. Rev.* **2010**, *39*, 228−240.
(35) Dreyer, D. R.; Ruoff, R. S.; Bielawski, C. W. *Angew. Chem., Int. Ed.* **2010**, *49*, 9336−9344.
(36) Hirsch, A. *Angew. Chem., Int. Ed.* **2009**, *48*, 6594−6596.
(37) Olley, R. H.; Bassett, D. C. *Polymer* **1982**, *23*, 1707−1710.
(38) Zhao, X.; Chu, B. T. T.; Ballesteros, B.; Wang, W.; Johnston, C.; Sykes, J. M.; Grant, P. S. *Nanotechnology* **2009**, *20*, 065605−065613.
(39) Zhong, X. H.; Li, Y. L.; Liu, Y. K.; Qiao, X. H.; Feng, Y.; Liang, J.; Jin, J.; Zhu, L.; Hou, F.; Li, J. Y. *Adv. Mater.* **2010**, *22*, 692−696.
(40) Masarapu, C.; Zeng, H. F.; Hung, K. H.; Wei, B. *ACS Nano* **2009**, *3*, 2199−2206.
(41) Li, X.; Rong, J.; Wei, B. *ACS Nano* **2010**, *4*, 6039−6049.
(42) An, K. H.; Kim, W. S.; Park, Y. S.; Moon, J. M.; Bae, D. J.; Lim, S. C.; Lee, Y. S.; Lee, Y. H. *Adv. Funct. Mater.* **2001**, *11*, 387−392.
(43) Kim, J. H.; Nam, K. W.; Ma, S. B.; Kim, K. B. *Carbon* **2006**, *44*, 1963−1968.
(44) Du, C.; Yeh, J.; Pan, N. *Nanotechnology* **2005**, *16*, 350−353.
(45) Jurewicz, K.; Babeł, K.; Pietrzak, R.; Delpeux, S.; Wachowska, H. *Carbon* **2006**, *44*, 2368−2375.

(46) Jang, I. Y.; Muramatsu, H.; Park, K. C.; Kim, Y. J.; Endo, M. *Electrochem. Commun.* **2009**, *11*, 719−723.
(47) Niu, Z.; Zhou, W.; Chen, J.; Feng, G.; Li, H.; Ma, W.; Li, J.; Dong, H.; Ren, Y.; Zhao, D.; Xie, S. *Energy Environ. Sci* **2011**, *4*, 1440−1446.
(48) Lee, S. W.; Kim, B. S.; Chen, S.; Shao-Horn, Y.; Hammond, P. T. *J. Am. Chem. Soc.* **2009**, *131*, 671−679.
(49) Kaempgen, M.; Chan, C. K.; Ma, J.; Cui, Y.; Gruner, G. *Nano Lett.* **2009**, *9*, 1872−1876.
(50) Hiraoka, T.; Izadi-Najafabadi, A.; Yamada, T.; Futaba, D. N.; Yasuda, S.; Tanaike, O.; Hatori, H.; Yumura, M.; Iijima, S.; Hata, K. *Adv. Funct. Mater.* **2010**, *20*, 422−428.
(51) Hu, L.; Choi, J. W.; Yang, Y.; Jeong, S.; Mantia, F. L.; Cui, L. F.; Cui, Y. *Proc. Natl. Acad. Sci. U.S.A.* **2009**, *106*, 21490−21494.